Japanese Journal of Applied Physics

REGULAR PAPER

Thermodynamic analyses of thermal evaporation of $BaSi_2$

Japanese Journal of Applied Physics **59**, SFFA02 (2020) **REGULAR PAPER**
https://doi.org/**10.7567/1347-4065/ab5b64**

Thermodynamic analyses of thermal evaporation of $BaSi_2$

Kosuke O. Hara[1*], Keisuke Arimoto[1], Junji Yamanaka[2], and Kiyokazu Nakagawa[1]

[1]*Center for Crystal Science and Technology, University of Yamanashi, Kofu, Yamanashi 400-8511, Japan*
[2]*Center for Instrumental Analysis, University of Yamanashi, Kofu, Yamanashi 400-8510, Japan*

[*]E-mail: khara@yamanashi.ac.jp

Received August 29, 2019; accepted November 25, 2019; published online January 17, 2020

Thermal evaporation is a useful method for the deposition of high-quality photovoltaic $BaSi_2$ films. The elemental processes of $BaSi_2$ film formation are, however, complicated due to vapor composition change during $BaSi_2$ evaporation. In this study, we thermodynamically calculate the vapor composition for quantitative explanation of the evaporation process. The Ba and Si vapor fluxes are calculated from relative partial molar enthalpies of Ba and Si in Ba–Si melt. Calculations show a tendency of decreasing Ba vapor flux and increasing Si flux with decreasing mole fraction of Ba in Ba–Si melt, by which the vapor composition change from being Ba-rich to being Si-rich during thermal evaporation of $BaSi_2$ is successfully explained. The calculation results are discussed by comparing with the depth profiles of evaporated films deposited at room temperature and deposition rate. The present results would be useful as a theoretical basis of thermal evaporation of $BaSi_2$.

1. Introduction

$BaSi_2$ is an attractive photovoltaic material possessing excellent optical and minority-carrier properties.[1,2] The band gap of 1.3 eV is suitable for single-junction solar cells, while optical absorption coefficients exceed $10^4\,cm^{-1}$ for photon energies over the gap energy,[3–6] which enables thin-film device architectures. A long minority-carrier lifetime up to 27 μs when passivated suggests potential high performance as a photoabsorber layer material.[7–11] The abundance of constituent elements in the Earth's crust is another favorable feature of $BaSi_2$ toward large-scale terrestrial applications of solar cells. The highest power conversion efficiency among the solar cells using $BaSi_2$ is 9.9%, which was achieved by a p-type $BaSi_2$/n-type Si heterojunction.[12–14] $BaSi_2$ pn homojunction cells have also been realized recently.[15,16]

Thermal evaporation is a useful method for $BaSi_2$ film preparation.[17–19] High-quality $BaSi_2$ films can be obtained, as evidenced by a long minority-carrier lifetime up to 27 μs after AlO_x passivation and high photoresponsivity corresponding to an external quantum efficiency of 22%.,[6,10] while taking advantage of a high deposition rate up to 3 $\mu m\,min^{-1}$[20] and dry-air-stable source material. Elemental processes of $BaSi_2$ film formation by thermal evaporation are, however, complicated because the vapor composition of $BaSi_2$ differs from the melt, as is often the case with evaporation of alloys. In fact, the vapor is rich in Ba at the initial stage of evaporation, and it changes to being Si-rich.[17,21] In addition, since a part of Si in $BaSi_2$ melt segregates on the evaporation boat and reacts with the refractory metal boat,[18] the deposited film is abundant in Ba compared with the $BaSi_2$ source. Stoichiometric $BaSi_2$ films are, therefore, formed after enough diffusion and the reaction with a Si substrate.[19,21–23] The reason why the vapor composition changes with time is presumably because Ba with a higher vapor pressure evaporates faster than Si. It has, however, not been quantitatively explained on the basis of thermodynamic data. In this study, we elucidate the vapor composition change during $BaSi_2$ evaporation by calculating Ba and Si vapor fluxes using available thermodynamic data. It will be shown that the calculated vapor fluxes agree well with experimental observations.

2. Methods

2.1. Theoretical calculations

Two methods were employed for calculating the vapor fluxes of Ba and Si generated from $BaSi_2$ melt. The first method used relative partial molar enthalpies of Ba ($\overline{H}_{Ba}$) and Si ($\overline{H}_{Si}$) in liquid Ba–Si alloys at 1450 °C, reported by Esin et al.[24] Assuming the regular solution, activity coefficients of Ba (γ_{Ba}) and Si (γ_{Si}) are related with $\overline{H}_{Ba}$ and $\overline{H}_{Si}$ as

$$\overline{H}_i = RT \ln \gamma_i. \tag{1}$$

Here, i denotes Ba or Si. R and T are the gas constant and temperature, respectively. From γ_i and equilibrium vapor pressure of pure elements, activities (α_i) and partial vapor pressures of species i (p_i) are obtained. Then, the vapor fluxes of i (J_i) are derived using the following equation:

$$J_i = \frac{2.64 \times 10^{20} p_i}{\sqrt{M_i T}}\ cm^{-2}\,s^{-1}, \tag{2}$$

where M_i is the atomic weight of i.

The second method used Miedema's semi-empirical model[25] to calculate $\overline{H}_i$. Miedema's model enables to calculate the heat of formation for almost all binary alloys from basic properties such as molar volume, electronegativity, and electron density at the Wigner–Seitz cell boundary of elements in the systems. Recent data mining study dealing with 813 binary alloy systems also validated the capability of Miedema's theory to distinguish miscible and immiscible systems.[26] Using the calculated $\overline{H}_i$ values, J_i was calculated by the same procedure as the first method.

2.2. Experimental methods

Commercial $BaSi_2$ lumps (99% in purity, Kojundo Chemical Laboratory) were ground into granules of <5 mm in diameter. The $BaSi_2$ granules were placed on a tungsten boat in a vacuum chamber, and were evaporated by resistive heating of the boats. The base pressure of the chamber was below 1×10^{-3} Pa. The vapor was deposited on Ge(100) substrates at room temperature. The deposition rate was monitored by a quartz microbalance. Composition depth profiles of the

deposited films were analyzed by Auger electron spectroscopy (AES). Electron acceleration voltage was 10 kV.

3. Results and discussion

According to the phase diagram of the Ba–Si system reported by Pani and Palenoza,[27] $BaSi_2$ congruently melts at 1180 °C and constitutes an eutectic system with Si, the melting point of which is 1414 °C. The eutectic point is 1060 °C at a mole fraction of Ba (X_{Ba}) of 0.17. Esin et al. obtained the $\overline{H}_i$ data for X_{Ba} of 0–0.43 at 1450 °C, where the Ba–Si alloy is in a liquid state. Figure 1 summarizes the reported $\overline{H}_i$ values[24] and the α_i, and J_i values calculated from $\overline{H}_i$ (i = Ba or Si). In accordance with small $\overline{H}_{Ba}$ values, α_{Ba} is close to zero in the calculated X_{Ba} range. On the other hand, $\overline{H}_{Si}$ values close to zero in a X_{Ba} range of 0–0.1 brings about $\gamma_{Si} \sim 1$, leading to $\alpha_{Si} \sim X_{Si} = 1 - X_{Ba}$, which is consistent with Raoult's law. It is also noticed from the α_i data that α_i values are smaller than X_i, i.e. there is negative deviation, indicating that there is a chemical affinity between Ba and Si.

Figure 1(c) shows the calculated vapor fluxes at different melt compositions. Equilibrium vapor pressures of pure Ba and Si reported by Jacob and Waseda,[28] and Tomooka et al.[29] were used after extrapolation for the calculation. It is found that at X_{Ba} of 0.33, which is the composition of congruent $BaSi_2$ melt, J_{Ba} is by four orders of magnitude larger than J_{Si}. This means that Ba predominantly evaporates from $BaSi_2$ melt. During thermal evaporation of $BaSi_2$, thus, Ba first evaporates from the melt. As a result, X_{Ba} decreases. Then, J_{Ba} decreases while J_{Si} increases, according to Fig. 1(c). Finally, when $J_{Ba}/(J_{Ba} + J_{Si}) = X_{Ba}$ is reached, the melt and vapor compositions are fixed. Based on the data in Fig. 1, the final melt and vapor compositions are X_{Ba} of 0.19. That is, the vapor is rich in Si at the last stage of evaporation. Therefore, the change of vapor composition from being Ba-rich to being Si-rich during thermal evaporation of $BaSi_2$ is well explained by theoretical calculations.

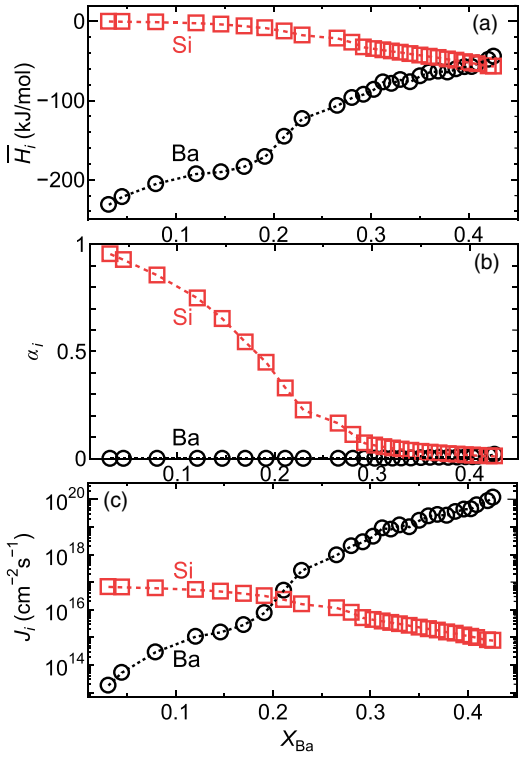

Fig. 1. (Color online) (a) The $\overline{H}_i$ values at 1450 °C reported by Esin et al.[24] and (b) the α_i, and (c) J_i values calculated from $\overline{H}_i$ (i = Ba or Si).

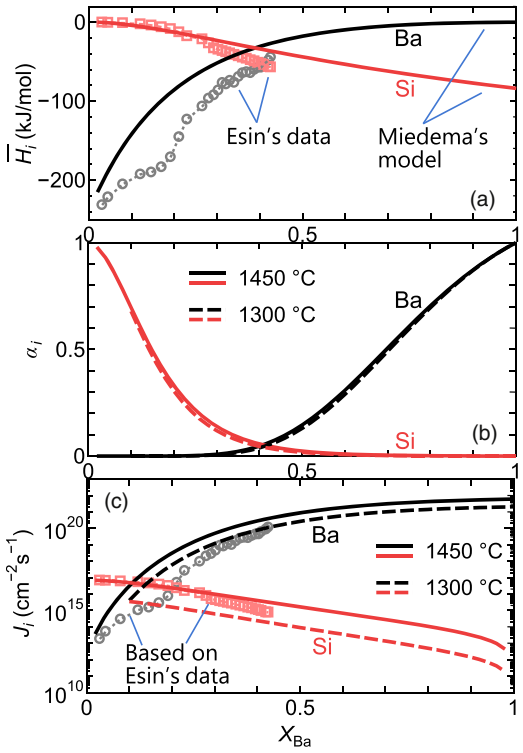

Fig. 2. (Color online) (a) The $\overline{H}_i$, (b) α_i, and (c) J_i values calculated by Miedema's model (i = Ba or Si).

Figure 2 summarizes the $\overline{H}_i$, α_i, and J_i values at 1450 °C and 1300 °C, calculated by Miedema's model. Because $\overline{H}_i$ does not depend on temperature in Miedema's model, one set of data is shown in Fig. 2(a), together with the data reported by Esin et al.[24] The $\overline{H}_{Ba}$ values calculated by Miedema's model are by several tens kJ/mol larger than the experimental values by Esin et al.[24] while $\overline{H}_{Si}$ values are similar. The overall tendency of $\overline{H}_i$ values against X_{Ba} is similar. One of the merits using Miedema's model is the capability of seeing the tendency in a wide composition range and at different temperatures. α_i values at 1450 °C and 1300 °C are shown in Fig. 2(b). At 1300 °C, Ba–Si melt equilibrates with solid Si for X_{Ba} = 0–0.08, where the present calculation is not applicable. This is why the data of 1300 °C in this X_{Ba} range are not displayed. The difference between different temperatures is small. Comparing with Fig. 1, it is found that the α_i values calculated by Miedema's model agree well with those based on the $\overline{H}_i$ values by Esin et al.[24]

Calculated J_i values are displayed in Fig. 2(c). A tendency of increasing J_{Ba} and decreasing J_{Si} is found as X_{Ba} increases, which is similar to Fig. 1(c). Therefore, the vapor composition change from being Ba-rich to Si-rich can be explained also by the calculation based on Miedema's model. A difference is larger J_{Ba} values than those based on Esin's data, which derives from the difference in $\overline{H}_{Ba}$ [Fig. 2(a)]. Due to the difference in J_{Ba}, the final melt and vapor compositions during thermal evaporation are different. Based on Miedema's model, the final compositions are X_{Ba} of 0.07, which are smaller than those based on Esin's data. At 1300 °C, J_i values are lower than those at 1450 °C mainly due to lower equilibrium vapor pressures of pure Ba and Si. It is also noted that the J_{Ba} and J_{Si} curves do not cross in the

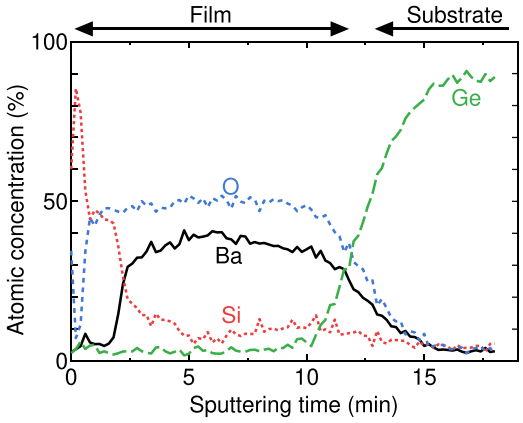

Fig. 3. (Color online) AES composition depth profiles of the film deposited on a Ge(100) substrate by thermal evaporation of $BaSi_2$.

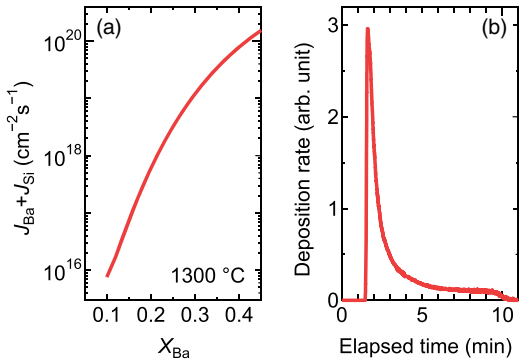

Fig. 4. (Color online) (a) Total vapor flux at 1300 °C, $J_{Ba} + J_{Si}$, calculated by Miedema's model. (b) Deposition rate during thermal evaporation of $BaSi_2$ measured by a quartz microbalance.

liquid range. This is because two phases equilibrate in a region of $X_{Ba} \leqslant 0.08$, where the melt composition is fixed at $X_{Ba} = 0.08$. As a result, J_{Ba} is larger than J_{Si} until the end of evaporation. Si remaining in the melt would segregate as a solid, which was previously observed on the boat after evaporation of $BaSi_2$.[18] Since the two phase region expands as temperature decreases, the amount of segregated Si would be larger and the average vapor composition would be more rich in Ba at lower temperatures, which supports our previous discussion on the effects of boat heating temperature on the structure and electrical properties of $BaSi_2$ films.[20,30]

To validate the calculation results, $BaSi_2$ was deposited on a Ge(100) substrate at room temperature by thermal evaporation and analyzed by AES. Boat heating current was 80 A, which corresponds to the temperature of 1300 °C measured by a radiation thermometer without emissivity correction when the source is not loaded. Figure 3 displays the composition depth profiles of the deposited film. After exposure to air, the film is oxidized, which is the reason of high oxygen concentration. It is possible that the depth profiles change through oxidation. However, the overall tendency that Ba concentration is high near the substrate and in the middle of the film while it is low near the surface agrees with the vapor composition change expected from calculated J_{Ba} and J_{Si} values in Figs. 1(c) and 2(c). The result that almost Si is deposited at last, however, does not agree with the calculation result that J_{Ba} is larger than J_{Si} for all X_{Ba} at 1300 °C [Fig. 2(c)]. This discrepancy is possibly due to the inaccuracy of the calculation and the underestimation of the boat temperature without emissivity correction.

It is also worth comparing the total vapor flux ($J_{Ba} + J_{Si}$) and deposition rate during thermal evaporation. The $J_{Ba} + J_{Si}$ values at 1300 °C calculated by Miedema's model are shown in Fig. 4(a). It is found that $J_{Ba} + J_{Si}$ decreases near-exponentially as X_{Ba} decreases. Figure 4(b) shows deposition rate during thermal evaporation of $BaSi_2$ with a boat heating current of 80 A. Because the vapor composition continuously changes, the rate calibration was not possible. It is, however, clearly observed that the deposition rate decreases near-exponentially after steep rise due to the current rise to 80 A. This decrease is presumably owing to the decrease in X_{Ba}, which leads to the decrease in $J_{Ba} + J_{Si}$, as understood from Fig. 4(a). This comparison is, actually, not under the same condition because the melt temperature deviates from 1300 °C for two reasons. One is the absence of emissivity correction for boat temperature measurement, which probably leads to underestimation of temperature. The other is the lowering of melt temperature during thermal evaporation due to the latent heat. However, the decreasing tendency of deposition rate is well explained by the melt composition change.

4. Conclusions

We have investigated the vapor fluxes during thermal evaporation of $BaSi_2$ by two theoretical calculations. One used measured $\overline{H_i}$ values while the other used calculated $\overline{H_i}$ values by Miedema's model. By both methods, tendencies of decreasing J_{Ba} and increasing J_{Si} with decreasing X_{Ba} are revealed, by which the vapor composition change from being Ba-rich to being Si-rich during thermal evaporation of $BaSi_2$ is well explained. The calculated tendencies of J_i have been validated by the composition depth profiles of the film deposited on a Ge(100) substrate at room temperature by thermal evaporation and its deposition rate. The present results can be a theoretical basis of the thermal evaporation of $BaSi_2$.

Acknowledgments

This work was partly supported by JSPS KAKENHI Grant Numbers JP16H03856 and JP17K14657, and Yashima Environment Technology Foundation.

ORCID iDs

Kosuke O. Hara https://orcid.org/0000-0001-6463-6540
Keisuke Arimoto https://orcid.org/0000-0002-3766-4324

1) T. Suemasu, Jpn. J. Appl. Phys. **54**, 07JA01 (2015).
2) T. Suemasu and N. Usami, J. Phys. D: Appl. Phys. **50**, 023001 (2016).
3) K. Toh, T. Saito, and T. Suemasu, Jpn. J. Appl. Phys. **50**, 068001 (2011).
4) N. A. A. Latiff, T. Yoneyama, T. Shibutami, K. Matsumaru, K. Toko, and T. Suemasu, Phys. Status Solidi C **10**, 1759 (2013).
5) M. Kumar, N. Umezawa, and M. Imai, Appl. Phys. Express **7**, 071203 (2014).
6) C. T. Trinh, Y. Nakagawa, K. O. Hara, R. Takabe, T. Suemasu, and N. Usami, Mater. Res. Express **3**, 076204 (2016).
7) K. O. Hara, N. Usami, K. Nakamura, R. Takabe, M. Baba, K. Toko, and T. Suemasu, Appl. Phys. Express **6**, 112302 (2013).
8) R. Takabe, K. O. Hara, M. Baba, W. Du, N. Shimada, K. Toko, N. Usami, and T. Suemasu, J. Appl. Phys. **115**, 193510 (2014).
9) T. Suhara, K. Murata, A. Navabi, K. O. Hara, Y. Nakagawa, C. T. Trinh, Y. Kurokawa, T. Suemasu, K. L. Wang, and N. Usami, Jpn. J. Appl. Phys. **56**, 05DB05 (2017).

10) N. M. Shaalan, K. O. Hara, C. T. Trinh, Y. Nakagawa, and N. Usami, Mater. Sci. Semicond. Process. **76**, 37 (2018).
11) Z. Xu et al., Phys. Rev. Mater. **3**, 065403 (2019).
12) D. Tsukahara, S. Yachi, H. Takeuchi, R. Takabe, W. Du, M. Baba, Y. Li, K. Toko, N. Usami, and T. Suemasu, Appl. Phys. Lett. **108**, 152101 (2016).
13) S. Yachi, R. Takabe, H. Takeuchi, K. Toko, and T. Suemasu, Appl. Phys. Lett. **109**, 072103 (2016).
14) T. Deng, T. Sato, Z. Xu, R. Takabe, S. Yachi, Y. Yamashita, K. Toko, and T. Suemasu, Appl. Phys Express **11**, 062301 (2018).
15) K. Kodama, R. Takabe, T. Deng, K. Toko, and T. Suemasu, Jpn. J. Appl. Phys. **57**, 050310 (2018).
16) K. Kodama, Y. Yamashita, T. Kaoru, and T. Suemasu, Appl. Phys. Express **12**, 041005 (2019).
17) Y. Nakagawa, K. O. Hara, T. Suemasu, and N. Usami, Jpn. J. Appl. Phys. **54**, 08KC03 (2015).
18) K. O. Hara, Y. Nakagawa, T. Suemasu, and N. Usami, Jpn. J. Appl. Phys. **54**, 07JE02 (2015).
19) K. O. Hara, K. Nakagawa, T. Suemasu, and N. Usami, Proc. Eng. **141**, 27 (2016).
20) K. O. Hara, C. T. Trinh, K. Arimoto, J. Yamanaka, K. Nakagawa, Y. Kurokawa, T. Suemasu, and N. Usami, J. Appl. Phys. **120**, 045103 (2016).
21) K. O. Hara, K. Arimoto, J. Yamanaka, and K. Nakagawa, J. Mater. Res. **33**, 2297 (2018).
22) K. O. Hara, J. Yamanaka, K. Arimoto, K. Nakagawa, T. Suemasu, and N. Usami, Thin Solid Films **595A**, 68 (2015).
23) K. O. Hara, C. Yamamoto, J. Yamanaka, K. Arimoto, K. Nakagawa, and N. Usami, Jpn. J. Appl. Phys. **57**, 04FS01 (2018).
24) Y. O. Esin, V. M. Sandakov, P. V. GELD, M. A. Ryss, A. K. Golev, and V. P. Zaiko, Zh. Prikl. Khim. **46**, 2402 (1973).
25) A. R. Miedema, P. F. De Chatel, and F. R. De Boer, Physica B **100**, 1 (1980).
26) R. F. Zhang, X. F. Kong, H. T. Wang, S. H. Zhang, D. Legut, S. H. Sheng, S. Srinivasan, K. Rajan, and T. C. Germann, Sci. Rep. **7**, 9577 (2017).
27) M. Pani and A. Palenzona, J. Alloys Compd. **454**, L1 (2008).
28) K. T. Jacob and Y. Waseda, J. Less-Common Met. **139**, 249 (1988).
29) T. Tomooka, Y. Shoji, and T. Matsui, J. Mass Spectrom. Soc. Jpn. **47**, 49 (1999).
30) K. O. Hara, K. Arimoto, J. Yamanaka, K. Nakagawa, and N. Usami, MRS Adv. **3**, 1387 (2018).